ASIAN JOURNAL OF CIVIL ENGINEERING (BHRC) VOL. 18, NO. 5(2017)
PAGE 837-852

# MODELLING THE RESPONSE OF TAPERED HEAD SLEEVE CONNECTION UNDER TENSILE LOAD USING FINITE ELEMENT METHOD

J. H. Ling*, Y. F. Liew, W. K. Leong and H. T. Sia
[1]School of Engineering and Technology, University College of Technology Sarawak, 96000 Sibu, Sarawak, Malaysia

**Received:** 24 September 2016; **Accepted:** 18 January 2017

## ABSTRACT

This paper presents a finite element analysis of the response of a grouted splice sleeve under tension. The connection is modelled in different bar embedded lengths (75, 125 and 175 mm) and sleeve diameters (50, 65 and 75 mm), and analysed by using ANSYS®. The results obtained include the load-displacement response, mechanical properties and failure mode. These results are verified with the experimental results, and found to have a variation exceeding ±10%. Nevertheless, based on the understandings obtained through modelling, the thickness and diameter of the sleeve can be reduced to 2.5 and 40 mm, respectively, to reduce the material cost by 60% without causing any decrease in the tensile capacity.

**Keywords:** Grouted splice sleeve; precast concrete connection; finite element analysis; tapered head sleeve.

## 1. INTRODUCTION

Grouted splice sleeve is a mechanical coupler used to connect steel bars. It has been widely used as the connection for precast concrete elements, such as wall panels [1-4], bridge assembly or pier caps [5-7], columns [8-10], beams[11, 12] and others. It is embedded in a precast concrete element during fabrication in the factories. At the construction site, it connects the structural elements by receiving the insertion of the reinforcing bars from the other component (Fig. 1).

*E-mail address of the corresponding author: lingjenhua@ucts.edu.my (J.H. Ling)

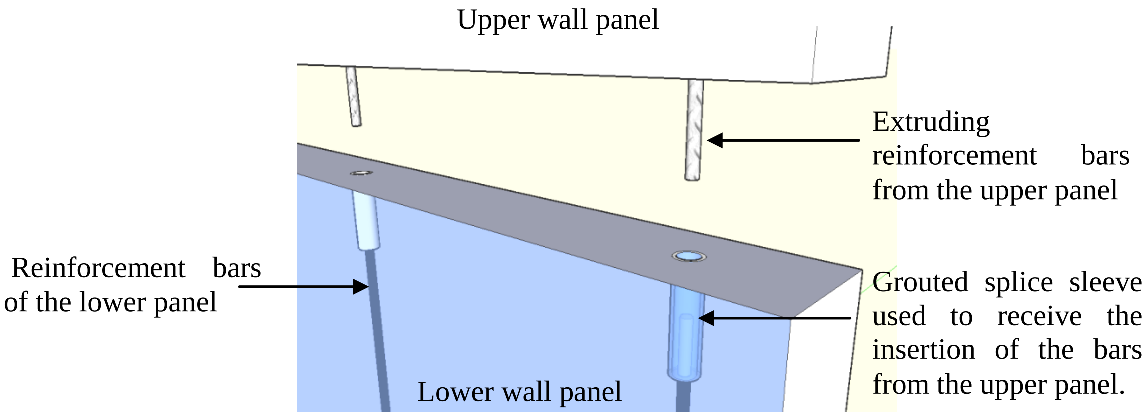


Figure 1. Grouted splice sleeve as the connection for precast concrete wall panels [13]

A typical grouted splice consists of two steel bars, a sleeve and some grout (Fig. 2). Steel bars are inserted and anchored in the sleeve. The bars are surrounded and bonded with non-shrink and high strength grout in the sleeve [14]. The interlocking mechanism between the bar ribs, the grout keys and the sleeve enables the connection to resist tensile load [15]. Under load, the sleeve provides confinement to the grout. It resists expansion of the grout and the propagation of the peripheral splitting cracks surrounding the spliced bars to ensure the bond is always in good condition [16]. For a typical grouted splice connection, about 8.5 to 16 times the bar diameter (8.5 – 16$d_b$) of bar embedded length is required for stresses to be fully transferred from one element to another [17].

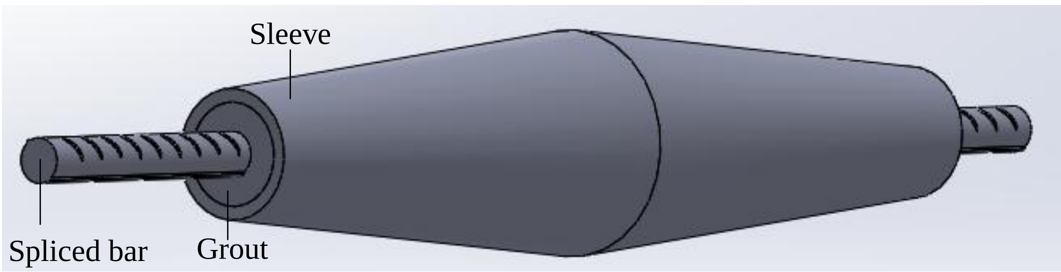


Figure 2. Components of a typical grouted splice

There are several grout splice sleeve available in the market, such as NMB Splice Sleeve®, Sleeve Lock®, and Lenton Interlok® [18]. Due to limited understanding, the designs and applications of grouted splice sleeves have been the works of specialists. In 1995, Einea et al. [19] proposed to connect steel bars using mild steel pipes with some modifications. Then, various materials and designs of the sleeve have been proposed by the researchers worldwide. These include mild steel pipes [15, 16, 18, 20, 21], high strength steel [22], aluminum tubes [8, 23], spirals [11, 24-27], square hollow sections [28], and glass fiber reinforced polymers [29-32]. Some even modify the spliced bars with enlarged heads to enhance its interlocking with the grout [13, 22].

The grouted splice specimens are usually tested with an incremental tensile load to determine the feasibility and the characteristic strength of the connection [28]. The parameters being studied include the bar embedded lengths, the sleeve or spiral diameters, the size of the spliced bars, the diameters of the bar head and the thickness of the sleeve [11, 14, 18, 22, 25].

The relevant standards specify a minimum tensile capacity of 125% of the nominal yield strength of the spliced bars [33, 34]. The behaviour of the grouted splice connection is generally evaluated based on the load-displacement [16, 21, 29], stress-strain responses [17, 22], bond-slip [30]. A good grouted splice connection shall offer (a) a high degree of stiffness, which is about equivalent to the stiffness of the steel bars, (b) a low bond-slip displacement, and (c) high post-yield ductility [20]. The design capacity is recommended to be not higher than the yielding strength obtained from the tensile load test.

Compared with the number of experimental studies, limited study has been carried out on numerically investigating the structural behaviour of grouted splice connection by using 3D finite element models. Thus far, we are aware of only one paper presenting such study which was done by Henin and Morcous (2015) [18].

This study investigates the response of Tapered Head Sleeve (THS) under tensile load by using the finite element method with the aid of a software ANSYS V14. The aim is to determine the feasibility of FEM to model the response of the connection and to propose an economical design for the connection design. The objectives and the scopes of this study are outlined in Table 1.

Table 1: Objectives and scope of study

| **Objectives** | **Scope** |
|---|---|
| O1: To investigate the behaviour of grouted splice sleeve connection under tensile load by using finite element modelling. | S1: Modelling of THS by using finite element method, with the aid of SolidWorks® and ANSYS® V14 software.<br>S2: Investigation of the responses, such as load-displacement curve, mechanical properties, stress developed at yield point and ultimate state, potential mode of failure. |
| O2: To compare the finite element modelling with the experimental result. | S3: Determination of the level of confidence of the predicting the response of the connection |
| O3: To propose an optimized design of the grouted splice connection by using the finite element model. | S4: The model is considered optimized based on the following assumption:<br>a. The stress contour of the grouted splice connection demonstrates a larger area undergoing a higher degree of stress as compared with the original design.<br>b. A significant decrease in the amount of material used (≥20% reduction in terms of cost) is found with an insignificant decrease in terms of structural performance (≤5% degradation in terms of ultimate capacity) of the proposed connection as compared with the original design |

## 2. METHODOLOGY

This study consists of the stages of (a) modelling the geometry and determining properties of the components and materials, (b) analysing the response of the connection under tensile load (obj. 1), (c) verifying the reliability of the analysed outcomes (obj. 2), and (d) optimizing the sleeve connection (obj. 3).

The geometry of THS was modelled by using SolidWorks® and the response under tensile load was simulated by using ANSYS® V14. The results are then compared with the experimental study [14] at the stages of pre-yield, yield and ultimate states in terms of the stiffness, yield strength, tensile capacity, displacements and failure mode.

The experimental results were obtained through tensile load test in the laboratory of Universiti Teknologi Malaysia, by using a 250 kN capacity Universal Testing Machine (Fig. 3). The details of the specimens and the test results are listed in Tables 2 and 3, respectively. However, in this study, only THS-2, 4, 5, 6 and 8 were modelled and analysed by using the Finite Element Method.

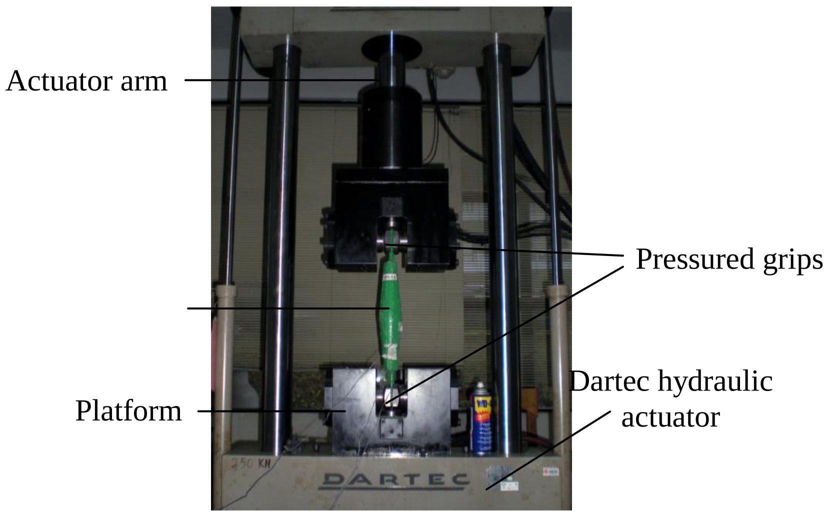


Figure 3. Tensile load test of Tapered Head Sleeve specimens

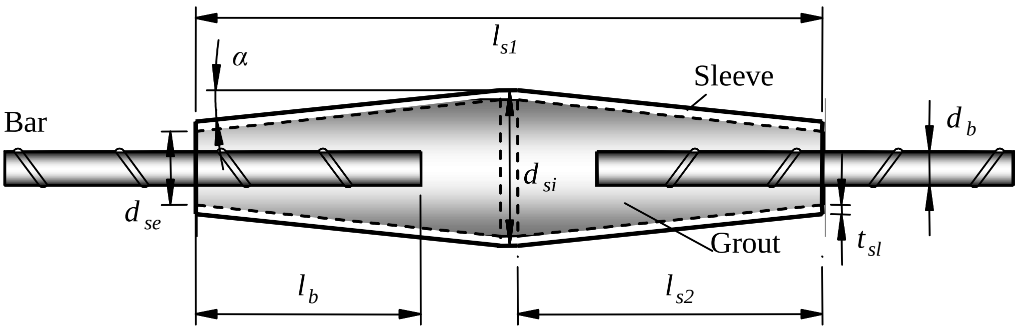


Figure 4. Configuration of Tapered Head Sleeve

Table 2: Dimensions of Tapered Head Sleeve (THS) (refer to Fig. 4)

| | Spliced Bar | | Sleeve | | | |
|---|---|---|---|---|---|---|
| Specimens | $d_b$ (mm) | $l_b$ (mm) | $d_{si}$ (mm) | $d_{se}$ (mm) | $l_{sl}$ (mm) | $t_{sl}$ (mm) |
| THS-1 | | | 50 | | | |
| THS-2 | | 75 | 65 | | | |
| THS-3 | | | 75 | | | |
| THS-4 | | | 50 | | | |
| THS-5 | 16 | 125 | 65 | 35 | 360 | 4.5 |
| THS-6 | | | 75 | | | |
| THS-7 | | | 50 | | | |
| THS-8 | | 175 | 65 | | | |
| THS-9 | | | 75 | | | |

Table 3: Test results of Tapered Head Sleeve (THS) specimens (average of three specimens)

| Specimen | Tensile capacity, $P_{u,avg}$ (kN) | Standard deviation of tensile capacity, $s_{1*}$ | Displacement at failure, $\delta_u$ (mm) | Standard deviation of displacement, $s_2$ (mm) | Failure mode |
|---|---|---|---|---|---|
| THS-1 | 112.2 | 5.59 | 3.6 | 1.31 | Bar bond-slip |
| THS-2 | 102.1 | 4.94 | 3.7 | 0.40 | Bar bond-slip |
| THS-3 | 96.1 | 6.13 | 3.4 | 0.38 | Bar bond-slip |
| THS-4 | 137.0 | 3.27 | 30.8 | 1.96 | Bar fracture |
| THS-5 | 135.4 | 2.34 | 30.3 | 0.59 | Bar fracture |
| THS-6 | 134.6 | 0.29 | 30.2 | 0.94 | Bar fracture |
| THS-7 | 137.7 | 3.40 | 25.9 | 1.13 | Bar fracture |
| THS-8 | 133.2 | 0.53 | 29.2 | 2.13 | Bar fracture |
| THS-9 | 135.5 | 0.71 | 26.5 | 1.11 | Bar fracture |

## 3. RESULTS AND DISCUSSIONS

### *3.1 Load-displacement response*

The behaviour of the Tapered Head Sleeve (THS) specimens under tensile load modelled by ANSYS 14 is presented in the load-displacement responses shown in Fig. 5(a) to (e). The mechanical properties as abstracted from these responses are presented in Table 4.

Table 4: Test results of THS

| Specimen | Stiffness, kN/mm | Yield strength, kN | Yield displacement, mm | Tensile capacity, kN | Ultimate displacement, mm | Ductility ratio | Failure mode |
|---|---|---|---|---|---|---|---|
| THS-2 | 35.0 | 105 | 3.00 | 105 | 4.41 | 1.47 | Bar Bond-slip |
| THS-4 | 40.0 | 110 | 2.75 | 110 | 4.55 | 1.66 | Bar Bond-slip |
| THS-5 | 37.9 | 110 | 2.90 | 110 | 5.35 | 1.84 | Bar Bond-slip |
| THS-6 | 26.3 | 105 | 4.00 | 105 | 4.51 | 1.13 | Bar Bond-slip |
| THS-8 | 58.5 | 117 | 2.00 | 140 | 44.86 | 22.43 | Bar Fracture |

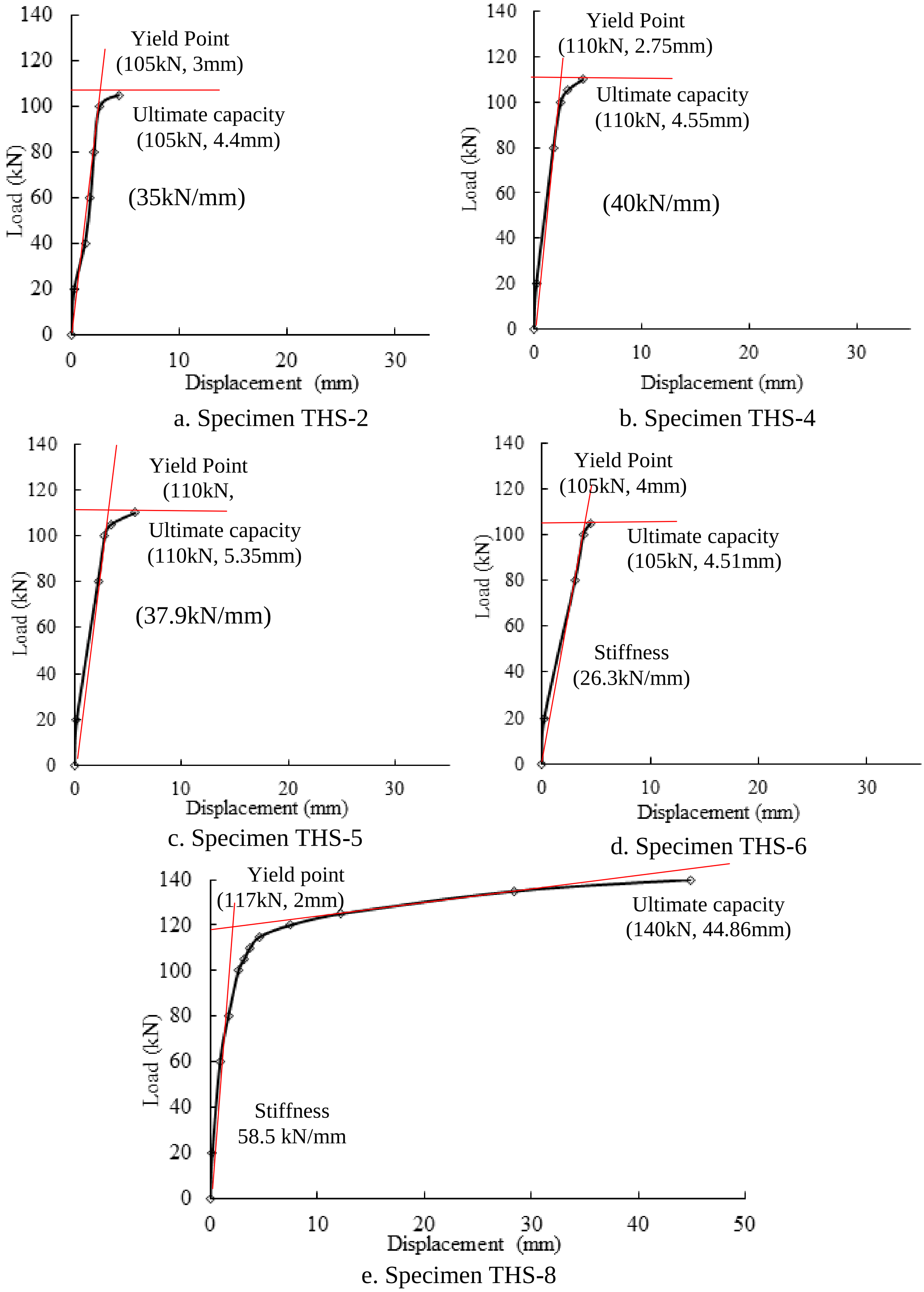


Figure 5. Load-displacement response of each specimen

Specimens THS-2, 4, 5 and 6 failed with a ductility ratio of less than 2 at about 110 kN load (Table 4). They failed with insignificant bar elongation (Fig. 6(a)) but with large displacement of about 5 mm towards the direction of load (Fig. 6(b)). The displacement was mainly due to failure of the bond and slippage of the spliced bar in the sleeve. It occurred prior to the completion of its yielding process, where the stresses in bars barely reached 500 N/mm$^2$ (Fig, 7). This demonstrates the response of a grouted splice connection when an inadequate bar embedded length is provided, where insufficient bond is generated in the sleeve to resist the pull-out force.

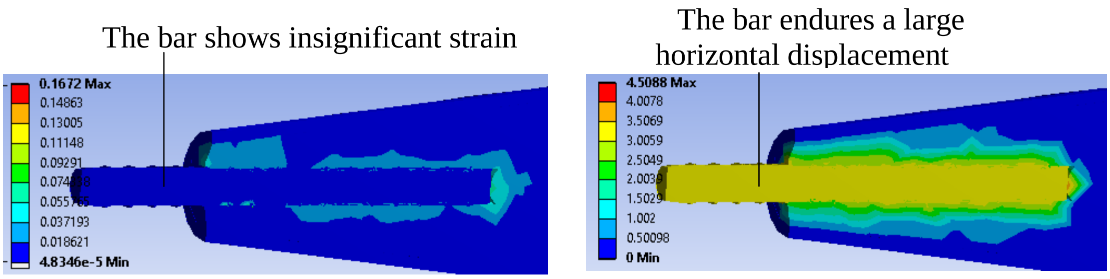


(a) Strain (mm/mm) (a) Deformation (mm)

Figure 6. Comparison between strain and deformation in specimen THS-6

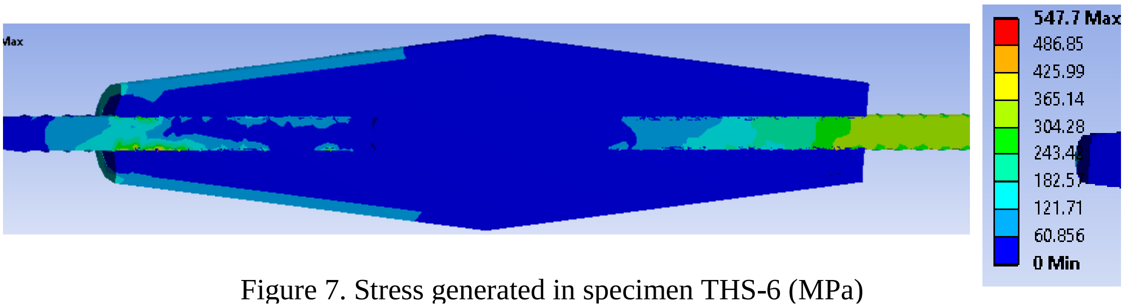


Figure 7. Stress generated in specimen THS-6 (MPa)

Specimen THS-8 failed at 140 kN load with a ductility ratio of 22.4. The spliced bar underwent a significant elongation prior to failure of the specimen (Fig. 8).

A high tensile stress accumulated in the spliced at a distance of about 1 to 2 times the bar diameter from the end of the sleeve (1 to 2$d_b$) (Fig. 9). The bar yielded (at about 117 kN), strain hardened, endured a necking process, elongated significantly and eventually fractured. This response indicates a sufficient bond strength was generated in the sleeve to resist the pull-out force. This is mainly due to the provision of an adequate bar embedded length (175 mm in this case).

As for the sleeve, high stress developed at the mid length of the sleeve. The region was used to bridge the discontinuity of the spliced bar. The sleeve did not yield. A low stress of less than 250 N/mm$^2$ and an insignificant strain were detected in the region (Figs. 8 and 9).

THS-8 recorded a total displacement of 44.9 mm. It is mainly contributed to by the post-yielding elongation of the spliced bars. There could be contributed to by (a) the tensile elongation of the sleeve, (b) the bond-slip displacement of the spliced bar from the grout,

(iv) the deformation of the grout in the sleeve, and (v) the bond-slip deformation of the grout from the sleeve, although the effects were insignificant.

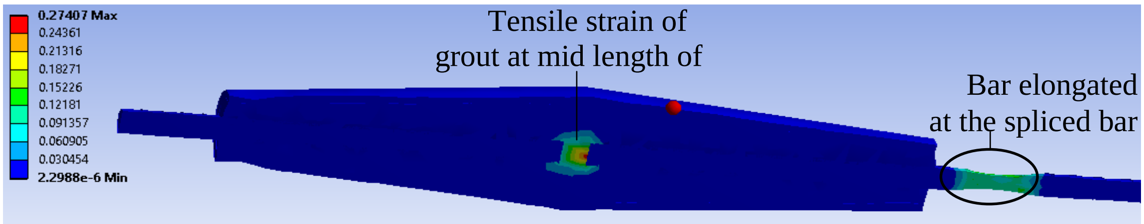


Figure 8. Strain developed in specimen THS-8 (mm/mm)

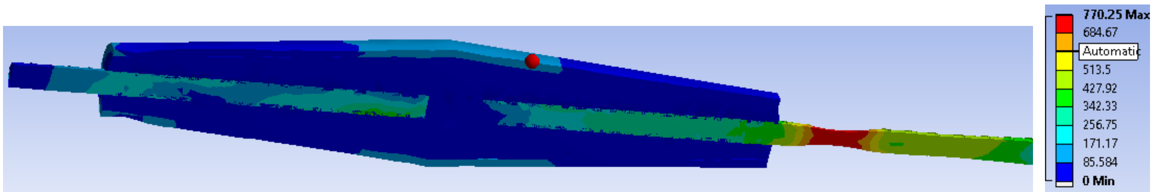


Figure 9. Stresses in specimen THS-8 (MPa)Grouted splice

*3.2 Parametric studies*

The effects of the two parameters as observed from the results are outlined as follows:

a. As the bar embedded length increases from 75 to 175 mm (about 5 to 11$d_b$):
- The connection stiffness increases by 67%.
- The yield strength increases by 10%.
- The ultimate strength increases by 33%.
- The ductility ratio increases by 1425%

b. As the sleeve diameter increases from 50 to 75 mm (about 3 to 5$d_b$):
- The connection stiffness reduces by 34%
- The yield strength decreases by 4.5%
- The ultimate strength decreases by 4.5%
- The ductility ratio reduces by 32%

In general, the effects of the sleeve diameter are less significant as compared with the bar embedded length. Nevertheless, based on these findings, a long bar embedded length and a small sleeve diameter are preferred when designing an effective grouted splice connection, especially for Tapered Head Sleeve connection.

*3.3 Result verifications*

The results obtained from the finite element model (FEM) analysis are compared and verified with the experimental results in the following aspects:

The closeness of the plots and trends of the predicted load-displacement curves are shown in Fig. 10 and the consistency of the responses, mechanical properties and failure mode at the pre-yield, yield and ultimate states are shown in Table 5.

Fig. 10 compares the load-displacement curve of each specimen, as obtained from FEM analysis, with the experimental results. The predicted load-displacement curves are about similar to the experimental results before the specimens yielded. However, FEM (a) predicted a larger displacement of the splice bars, and (b) gave a lower degree of the ductility as compared with the experimental results as observed from THS-4, 5 and 6.

Table 5 demonstrates the evaluation for determining the reliability of FEM to predict the responses of the grouted splice connection through comparison with the experimental results. The specimens are evaluated at the pre-yield, yielding and ultimate states, in the aspects of the connection's stiffness, yield strength, displacement at yield, tensile capacity, displacement at ultimate state and failure mode.

The reliability ratios, $R_r$, are computed by dividing the results from the finite element model with the experimental results. It quantifies the deviation of the predicted results from the experimental results. The specimens with $R_r$ ranging from 0.90 to 1.10 are considered acceptable. The finite element model is considered applicable for the respective specimens when at least 4 out of 6 aspects are considered acceptable.

Table 5: Comparison of the finite element analysis results with the experimental results

| Evaluation Criteria | | | Specimens | | | | |
|---|---|---|---|---|---|---|---|
| | | | **THS-2** | **THS-4** | **THS-5** | **THS-6** | **THS-8** |
| Pre-Yield State | Stiffness (kN/mm) | FEM | 35 | 40 | 37.9 | 26.3 | 58.5 |
| | | Exp. | 41.6 | 54.1 | 49 | 49.2 | 52.1 |
| | Reliability ratio, $R_r$ | | 0.84 | 0.74 | 0.77 | 0.53 | 1.12 |
| | Reliability | | X | X | X | X | X |
| Yielding State | Yield strength, $P_y$ (kN) | FEM | 105 | 110 | 110 | 105 | 117 |
| | | Exp. | 105.7 | 115.6 | 115.6 | 112.8 | 110.8 |
| | Reliability ratio, $R_r$ | | 0.99 | 0.95 | 0.95 | 0.93 | 1.06 |
| | Reliability | | √ | √ | √ | √ | √ |
| | Disp.at yield (mm) | FEM | 3 | 2.75 | 2.9 | 4 | 2 |
| | | Exp. | 2.5 | 2.2 | 2.4 | 2.4 | 2.2 |
| | Reliability ratio, $R_r$ | | 1.2 | 1.25 | 1.21 | 1.67 | 0.91 |
| | Reliability | | X | X | X | X | √ |
| Ultimate State | Tensile Capacity, $P_u$ (kN) | FEM | 105 | 110 | 110 | 105 | 140 |
| | | Exp. | 105.7 | 137 | 135.4 | 134.6 | 133.2 |
| | Reliability ratio, $R_r$ | | 0.99 | 0.8 | 0.81 | 0.78 | 1.05 |
| | Reliability | | √ | X | X | X | √ |
| | Total disp. (mm) | FEM | 4.41 | 4.55 | 5.35 | 4.51 | 44.86 |
| | | Exp. | 4.1 | 28.6 | 30 | 31.3 | 27.4 |
| | Reliability ratio, $R_r$ | | 1.08 | 0.16 | 0.18 | 0.14 | 1.64 |
| | Reliability | | √ | X | X | X | √ |
| | Failure Mode | FEM | Bar Bond-slip | Bar Bond-slip | Bar Bond-slip | Bar Bond-slip | Bar Fracture |
| | | Exp. | Bar Bond-slip | Bar Fracture | Bar Fracture | Bar Fracture | Bar Fracture |
| | Reliability | | √ | X | X | X | √ |
| | **Applicability** | | **A** | **NA** | **NA** | **NA** | **A** |

*Note: A – Applicable (at least four "√"), NA – Non-Applicable (less than four "√").

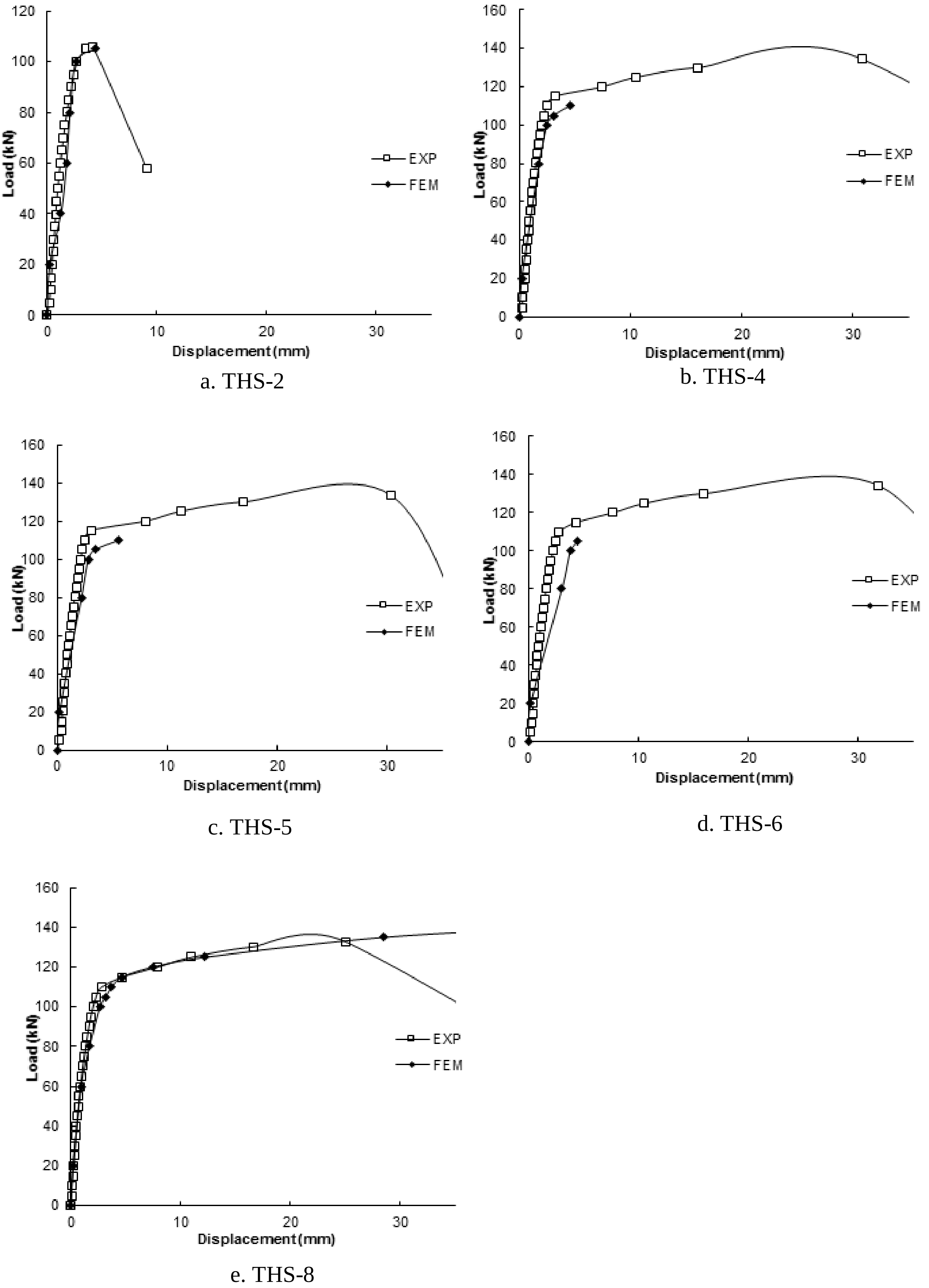


Figure 10. Comparison of the load-displacement response between the finite element analysis and the experimental results

From Fig. 10 and Table 5, the following is observed:

a. The finite element model could only predict the yield point of the grouted splice connection with the accuracy of ±7% (Table 5). The predictions in the other aspects such as stiffness, displacements, tensile capacity and the failure mode are beyond the acceptable range of ±10%.
b. Prior to achieving the yield strength, the finite element model generally gives a larger displacement and a lower tensile resistance as compared with the experimental results (Fig. 10). However, as the model predicted that THS-4, 5 and 6 to fail prematurely prior to completion of the yield process of the spliced bars, the total displacement at the ultimate state are generally not more than 20% of the experimental results.
c. The finite element model predicted THS-4, 5 and 6 to fail by bar bond-slip failure in a brittle manner. This contradicts the experimental results with bar fracture failure in a ductile manner.
d. The finite element model indicates that 125 mm bar embedded length ($\approx 8d_b$) is inadequate to generate sufficient bond strength to prevent the bar from being pulled out of the sleeve. However, based on the experimental results, the provided bar embedded length was sufficient.
e. The reliability ratio for the prediction of the ultimate capacity ranges from 0.78 to 1.05. The prediction is beyond the acceptable limits of ±10%.

The predicted outcomes deviate from the experimental results. This could be due to the following reasons:

a. Some factors that contribute to the load resisting mechanism of the grouted splice connection were omitted or not correctly modelled in this study. This includes (i) the mechanical interlocking interaction between the bar ribs and the grout keys in the sleeve, (ii) the surface friction between the bar and the grout, and (iii) the confining stress generated by the peripheral tensile resistance of the sleeve as the grout slipped towards the tapered end of the sleeve (Fig. 11).
b. The material properties of the connection used to do the simulation might not reflect the actual properties of the materials.
c. The model simulated the connection under an ideal condition, which is sometimes not achievable in the reality. For example (i) the bars are assumed to be perfectly aligned along the central axis of the sleeve without any eccentricity between the bars, (ii) the shape and dimension of the sleeve is precisely as per given in Table 2, (iii) the materials of the components of the connection are perfect, consistent and without any defect throughout the specimens, (iv) the interface between the sleeve and the grout is smooth, etc.

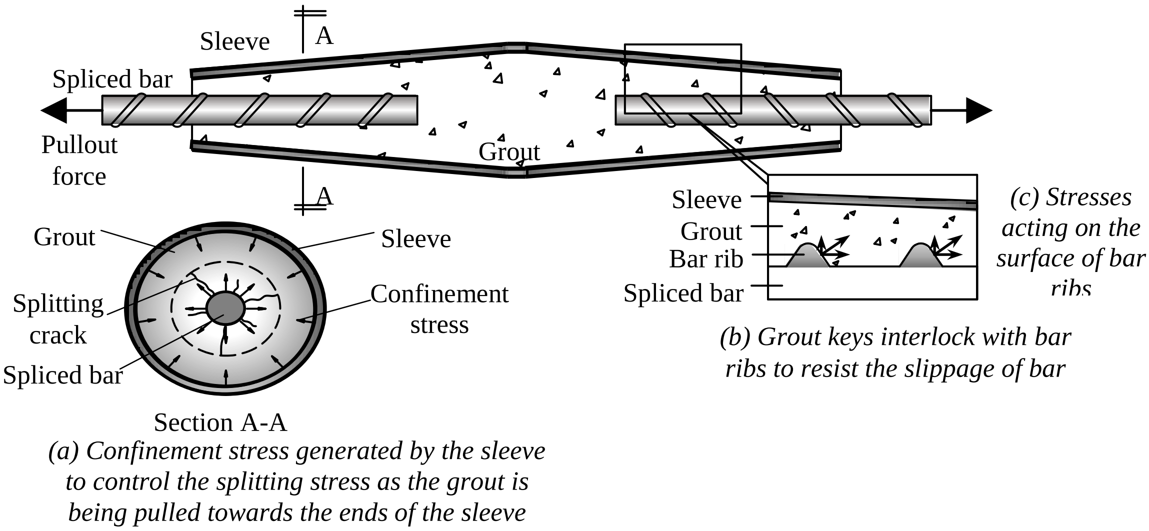


Figure 11. The load resisting mechanism of THS

To further refine the accuracy of the finite element model, the following is suggested:

a. To look into the material properties used in the model so that the response of the material could reflect the actual response more accurately.
b. To refine models in terms of the geometry of the components of the grouted splice connection, particularly the ribs on the spliced bars and the grout keys that interlock with the ribs.

However, a comparative study could still be done for the optimization purposes by comparing the models using the same set of assumptions and procedures.

*3.4 Optimization*

The optimization was carried out with reference to specimen THS-5. For specimen THS-5.1, the thickness of the sleeve was reduced to 2.5 mm and for THS-5.2, the sleeve diameters were reduced to 40 and 30 mm for $d_{si}$ and $d_{se}$, respectively.

The results show that there is no reduction in terms of tensile strength after the optimization (Table 6 and Fig. 12). The sleeve is used more efficiently, where a larger area of the sleeve is having a higher degree of stress compared with the initial design. The area is estimated to grow from about 30% to 80% after optimization (Table 7). The cost of the connection is reduced by about 60% (Table 7).

Table 6: The ultimate strength and displacement of optimized connection

| Specimen | Ultimate tensile strength, kN | Differences (%)* | Ultimate displacement, mm | Differences (%) |
|---|---|---|---|---|
| THS-5 | 110 | | 5.35 | |
| THS-5.1 | 110 | 0 | 5.48 | + 2.5 |
| THS-5.2 | 110 | 0 | 5.08 | - 5 |

Note: The differences are with respect to THS-5.

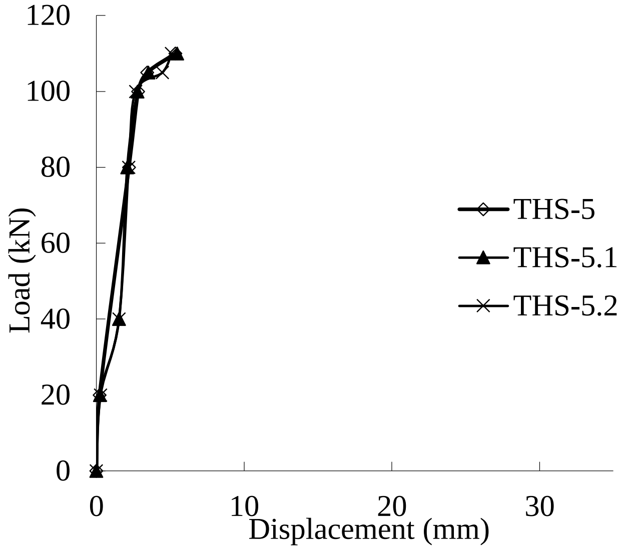


Figure 12. Comparison of load-displacement curves of optimization trials with THS-5

Table 7: Comparison of the optimization outcomes

| | THS-5 (Original) | | | THS-5.1 (First trial) | | | THS-5.2 (Second trial) | | |
|---|---|---|---|---|---|---|---|---|---|
| Components | Grout | Sleeve | Bar | Grout | Sleeve | Bar | Grout | Sleeve | Bar |
| Max stress (N/mm$^2$) | - | - | 586 | - | - | 568 | - | - | 568 |
| Stress contour | 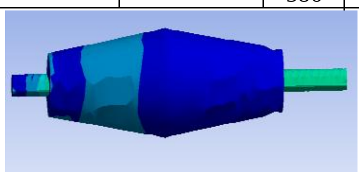 ≈ 30% coverage | | | 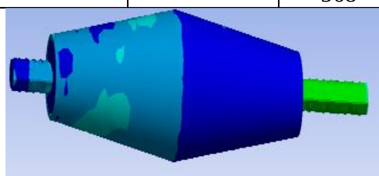 ≈ 50% coverage | | | 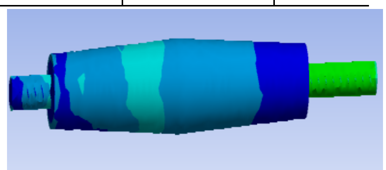 ≈ 80% coverage | | |
| Material volume (mm$^3$) | $6.7 \times 10^5$ | $2.76 \times 10^5$ | - | $6.7 \times 10^5$ | $1.48 \times 10^5$ | - | $3.06 \times 10^5$ | $1.06 \times 10^5$ | - |
| Mass (kg/unit) | 1.48 | 2.17 | - | 1.48 | 1.16 | - | 0.68 | 0.84 | - |
| Cost (RM/unit) | 1.78 | 8.68 | - | 1.78 | 4.64 | - | 0.81 | 3.34 | - |
| Total cost (RM/unit) | 10.46 | | - | 6.42 | | - | 4.15 | | - |

*Note: The cost is computed based on the following values, as given by Ling (2016):

a. Densities of steel and grout are 7850 and 2200 kg/m$^3$, respectively
b. Costs of steel and grout are approximately RM4.00 and RM1.20, respectively.

## 4. CONCLUSION

This study uses SolidWork® and Ansys® software to model and perform a finite element analysis on a grouted splice connection called Tapered Head Sleeve (THS). The response of the connection with different sleeve diameter and bar embedded length under incremental tensile load was studied. The results were then verified based on the experimental results.

The modelling results show that:

a. The connection can fail by bar bond-slip or bar fracture failure, depending on the adequacy of the bar embedded length.
b. The deformation of the connection at the ultimate state is mainly contributed to by (i) the elongation of the spliced bars when sufficient bond strength is provided, and (ii) bar bond-slip displacement with insufficient bond strength.
c. An increase in the bar embedded length from 5 to $11d_b$ increases the connection stiffness, yield strength and ultimate strength by 67%, 10%, and 33%, respectively. As the sleeve diameter increases from 3 to $5d_b$, the connection stiffness, yield strength and ultimate strength reduce by 34%, 4.5% and 4.5%, respectively. For this, the effects of sleeve diameter are less significant compared with bar embedded length.

At the moment, the model is still unable to accurately predict the response of the grouted splice connection in most of the aspects. The reliability ratio exceeded the acceptable limits of ±10%. With this limitation, the study proceeds with the attempts to optimize the grouted splice connection proposed by Ling (2016) based on the model developed.

By reducing the thickness and the diameters of the sleeve to 2.5 mm and 40 mm, respectively, the grouted splice connection is expected to resist tensile load at about 60% cost reduction. Noting the fact that the FEM predictions deviated from the experimental results, the findings regarding the optimized design as proposed in this study need to be further verified and confirmed through an experimental study.

## REFERENCES

1. Zhu Z, Guo Z. Experiments on hybrid precast concrete shear walls emulating monolithic construction with different amounts of posttensioned strands and different debond lengths of grouted reinforcements, *Advances in Materials Science and Engineering*, **2016**(2016) 13 p.
2. Qiong Y, Xin G, Yongqing F, Zhiyuan X, Xilin L. Grouted sleeve lapping connector and component performance tests, *Revista Tecnica de la Facultad de Ingenieria Universidad del Zulia*, No. 6, **39**(2016) 136-45.
3. Qiong Y, Kun X, Zhiyuan X, Yongqing F, Xilin L. Seismic *Behavior of Precast Shear Walls with Vertical Reinforcements Overlap Grouted in Constraint Sleeve*, *Revista Tecnica de la Facultad de Ingenieria Universidad del Zulia*, **39**(2016) 207-17.
4. Yajun L, Naiyan G. Tests on seismic behavior of pre-cast shear walls with vertical reinforcements spliced by two different grout ways, *The Open Civil Engineering Journal*, **9**(2015) 382-87.
5. Parks JE, Papulak T, Pantelides CP. Acoustic emission monitoring of grouted splice sleeve connectors and reinforced precast concrete bridge assemblies, *Construction and Building Materials*, **122**(2016) 537-47.
6. Redd SC. Strength, durability, and application of grouted couplers for integral abutments in accelerated bridge construction projects: IOWA state university, 2016.
7. Ameli MJ, Parks JE, Brown DN, Pantelides CP. Seismic evaluation of grouted splice

sleeve connections for reinforced precast concrete column – to - cap beam joints in accelerated bridge construction, PCI Journal, **60**(2015) 80-103.
8. Tullini N, Minghini F. Grouted sleeve connections used in precast reinforced concrete construction – Experimental investigation of a column-to-column joint, *Engineering Structures*, **127**(2016) 784-803.
9. Haber ZB, Saiidi MS, Sanders DH. Seismic Performance of Precast Columns with Mechanically Spliced Column-Footing Connections, *ACI Structural Journal*, **111**(2014) 1-12.
10. Belleri A, Riva P. Seismic performance and retrofit of precast concrete grouted sleeve connections, *PCI Journal*, **57**(2012) 97-109.
11. Sayadi AA, Rahman ABA, Jumaat MZB, Johnson Alengaram U, Ahmad S. The relationship between interlocking mechanism and bond strength in elastic and inelastic segment of splice sleeve, *Construction and Building Materials*, **55**(2014) 227-37.
12. A Sayadi A, Abd Rahman AB, Jumaat MZ, Alengaram UJ, Ahmad S. The relationship between interlocking mechanism and bond strength in elastic and inelastic segment of splice sleeve, *Construction and Building Materials*, **55**(2014) 227-37.
13. Loh HY. Development of Grouted Splice Sleeve and Its Performance under Axial Tension, Skudai, Johor, Universiti Teknologi Malaysia, 2008.
14. Ling JH, Abd Rahman AB, Ibrahim IS, Abdul Hamid Z. Tensile capacity of grouted splice sleeves. *Engineering Structures*, **111**(2016) 285-96.
15. Alias A, Zubir MA, Shahid KA, Abd Rahman AB. Structural performance of grouted sleeve connectors with and without transverse reinforcement for precast concrete structure, *Procedia Engineering*, **53**(2013) 116-23.
16. Ling JH, Abd. Rahman AB, Ibrahim IS, Abdul Hamid Z. Behaviour of grouted pipe splice under incremental tensile load, *Construction and Building Materials*, **33**(2012) 90-8.
17. Haber ZB, Saiidi MS, Sanders DH. Behavior and simplified modeling of mechanical reinforcing bar splices, *ACI Structural Journal*, **112**(2015) 179-88.
18. Henin E, Morcous G. Non-proprietary bar splice sleeve for precast concrete construction, *Engineering Structures*, **83**(2015) 154-62.
19. Einea A, Yamane T, Tadros MK. Grout-Filled Pipe Splices for Precast Concrete Construction, *Precast/Prestressed Concrete Institute Journal*, **40**(1995) 82-93.
20. Abd Rahman AB, Ling JH, Ibrahim IS, Abd. Hamid Z. Performance of Grouted Sleeve Connectors Subjected to Incremental Tensile Loads, *Malaysian Construction Research Journal (MCRJ)*, **6**(2010) 39-55.
21. Alias A, Sapawi F, Kusbiantoro A, Zubir MA, Abd. Rahman AB. Performance of grouted splice sleeve connector under tensile load, *Journal of Mechanical Engineering and Sciences (JMES)*, **7**(2014) 1096-1102.
22. Seo SY, Nam BR, Kim SK. Tensile strength of the grout-filled head-splice-sleeve, *Construction and Building Materials*, **124**(2016) 155-66.
23. Ling JH, Abd Rahman AB, Abd. Hamid Z. Failure modes of aluminium sleeve under direct tensile load. *3rd International Conference on Postgraduate Education (ICPE-3)*, Penang, Sarawak Universiti Sains Malaysia (USM), 2008.
24. Aldin Hosseini SJ, Abd Rahman AB. Analysis of spiral reinforcement in grouted pipe

splice connectors, *Građevinar*, 65(2013) 537-46.
25. Aldin Hosseini SJ, Abd Rahman AB. Effects of spiral confinement to the bond behavior of deformed reinforcement bars subjected to axial tension, *Engineering Structures*, **112**(2016) 1-13.
26. Aldin Hosseini SJ, Abd. Rahman AB, Osman MH, Saim A, Adnan A. Bond behavior of spirally confined splice of deformed bars in grout, *Construction and Building Materials*, **80**(2015) 180-94.
27. Hosseini SJA, Rahman ABA. Analysis of spiral reinforcement in grouted pipe splice connectors, *Građevinar*, **65**(2013) 537-46.
28. Ling JH, Abd Rahman AB, Ibrahim IS. Feasibility study of grouted splice connector under tensile load, *Construction and Building Materials*, **50**(2014) 530-9.
29. A Sayadi A, Abd Rahman AB, Sayadi A, Bahmani M, Shahryari L. Effective of elastic and inelastic zone on behavior of glass fiber reinforced polymer splice sleeve, *Construction and Building Materials*, **80**(2015) 38-47.
30. Koushfar K, Abd Rahman AB, Ahmad Y. Bond behavior of the reinforcement bar in glass fiber-reinforced polymer connector. Građevinar, **66**(2014) 301-10.
31. Tastani SP. Experimental evaluation of direct tension - pullout bond test, *International Symposium "Bond in Concrete - from Research to Standard"*, Budapest, 2002.
32. Tibbetts AJ, Oliva MG, Bank LC. Durable fiber reinforced polymer bar splice connections for precast concrete structures, *Composites & Polycon*, 2009.
33. ACI-318. Building Code Requirements for Structural Concrete and Commentary. Farmington Hills MI: American Concrete Institute, 2002.
34. AC-133. Acceptance Criteria for Mechanical Connector Systems for Steel Reinforcing Bars. ICC Evaluation Service, Inc, 2008.